Journal of *Marine Science and Engineering*

MDPI

Article

Arctic Nearshore Sediment Dynamics—An Example from Herschel Island—Qikiqtaruk, Canada

Boris Radosavljevic [1,2,*], Hugues Lantuit [1,2], Christian Knoblauch [3], Nicole Couture [4], Ulrike Herzschuh [1,2,5] and Michael Fritz [1]

1 Alfred Wegener Institute, Helmholtz Centre for Polar and Marine Research, 14473 Potsdam, Germany
2 Institute of Geosciences, University of Potsdam, 14476 Potsdam, Germany
3 Institute of Soil Science, University of Hamburg, 20148 Hamburg, Germany
4 Northern Canada Division, Geological Survey of Canada, Natural Resources Canada, Ottawa, ON K1A 0E7, Canada
5 Institute of Biochemistry and Biology, University of Potsdam, 14476 Potsdam, Germany
* Correspondence: boris.radosavljevic@gmail.com

Abstract: Increasing arctic coastal erosion rates imply a greater release of sediments and organic matter into the coastal zone. With 213 sediment samples taken around Herschel Island—Qikiqtaruk, Canadian Beaufort Sea, we aimed to gain new insights on sediment dynamics and geochemical properties of a shallow arctic nearshore zone. Spatial characteristics of nearshore sediment texture (moderately to poorly sorted silt) are dictated by hydrodynamic processes, but ice-related processes also play a role. We determined organic matter (OM) distribution and inferred the origin and quality of organic carbon by C/N ratios and stable carbon isotopes $\delta^{13}C$. The carbon content was higher offshore and in sheltered areas (mean: 1.0 wt.%., S.D.: 0.9) and the C/N ratios also showed a similar spatial pattern (mean: 11.1, S.D.: 3.1), while the $\delta^{13}C$ (mean: −26.4‰ VPDB, S.D.: 0.4) distribution was more complex. We compared the geochemical parameters of our study with terrestrial and marine samples from other studies using a bootstrap approach. Sediments of the current study contained 6.5 times and 1.8 times less total organic carbon than undisturbed and disturbed terrestrial sediments, respectively. Therefore, degradation of OM and separation of carbon pools take place on land and continue in the nearshore zone, where OM is leached, mineralized, or transported beyond the study area.

Keywords: permafrost; Arctic Ocean; stable carbon isotopes; nitrogen; sediment chemistry; sediment dynamics; Beaufort Sea; grain size

Citation: Radosavljevic, B.; Lantuit, H.; Knoblauch, C.; Couture, N.; Herzschuh, U.; Fritz, M. Arctic Nearshore Sediment Dynamics—An Example from Herschel Island—Qikiqtaruk, Canada. *J. Mar. Sci. Eng.* **2022**, *10*, 1589. https://doi.org/10.3390/jmse10111589

Academic Editor: Antoni Calafat

Received: 30 August 2022
Accepted: 11 October 2022
Published: 27 October 2022

1. Introduction

Approximately 4.9 to 14.0 Tg of particulate organic carbon (OC) are discharged into the Arctic Ocean via coastal erosion annually [1]—on the same order of magnitude as the annual amount discharged by rivers [2]. Arctic coasts are increasingly vulnerable to erosion [3–5], which is reflected in increasing coastal retreat rates across the Arctic [6–9]. Large stretches of the Arctic Ocean coastline are composed of ice-bonded permafrost soils containing 1.09 to 5.70% OC by weight [10]. Increasing coastal erosion, permafrost degradation, and river discharge are expected to lead to growing carbon and sediment fluxes with potential positive feedback to climate change [11–18]. These changes will also affect local ecosystems and sustenance activities of arctic communities [19] because additional nutrients may stimulate primary production [20], while turbidity associated with increased sediment load may decrease it [21,22]. The nearshore zone of the Arctic Ocean (<20 m depth) accounts for 7.5% of the total ocean and 20% of the shelf area [19,23]. However, there are only a few studies focusing on sediment characteristics and dynamics in the arctic nearshore zone and none with a high spatial resolution <5 km offshore.

The nearshore is a locus of various biogeochemical and physical processes that augment the degradation of terrestrial organic matter (OM). These include fungal and microbial decay [24,25], UV aided oxidation [26], and physical reworking through waves and ice-related processes. In the Beaufort Sea, all areas between 5 and 10 m water depths are subject to at least moderate wave dissipation rates, i.e., wave resuspension and reworking [27]. Terrestrial OM may undergo multiple episodes of cross-shore deposition and re-suspension. Ice-related processes are important physical agents in the Arctic. The entire Alaskan Beaufort Shelf is reworked by ice scouring over a 50-year period [28]. Changing ice cover conditions, especially late in the open-water season when the strongest storms occur, will cause more resuspension of bottom sediments [29]. Frequently resuspended 'fluid mud layers', like in our study area [30], are sites of highly effective OM degradation because oxic and anoxic conditions alternate and degradation is enhanced ('primed') by the addition of fresh marine OM [31]. Thus, the nearshore is an important site of terrestrial OM degradation.

Understanding the degradation dynamics of terrestrial OM in the nearshore requires a characterization and quantification of its sources, sinks and the transport mechanisms in the marine realm. A growing number of studies provides estimates of carbon fluxes from rivers and coastal erosion, characterizes the distribution of carbon and its provenance, or formulates carbon budgets [2,11,32–41]. The provenance and the state of degradation of OM is typically established by bulk geochemistry, stable carbon isotopes, radiocarbon dating, or biomarkers [39,42]. Few studies, however, described the sediment patterns and transport mechanisms in shelf areas of the Beaufort Sea [43–46].

The aforementioned studies, however, typically have a low spatial resolution, and with some exceptions are restricted to deeper shelf areas. Using sedimentological and bulk geochemical parameters, we aim to characterize nearshore sediments near Herschel Island—Qikiqtaruk in Yukon Territory, Canada. Our objective is to identify patterns of sediment and OM distribution around Herschel Island, including transport and degradation processes. In comparison with other studies, we want to deduce the fate of terrestrial organic carbon in this arctic nearshore environment at a high spatial resolution.

2. Study Area

We carried out our fieldwork in Thetis Bay (TB) and Workboat Passage (WBP) (Figure 1), which are nearshore areas close to Herschel Island—Qikiqtaruk (HI), Yukon Coast, Canada (69°36′ N; 139°04′ W) located in the southern Beaufort Sea. The island marks the farthest western advance of the Laurentide Ice Sheet during the Wisconsin glaciation [47–49] and consists of perennially frozen (i.e., permafrost) marine and terrestrial glacigenic sediments. The permafrost is contains widespread ground ice up to 60–70% by volume [50]. Herschel Island sediments contain considerable amounts of OC reaching up to 38.9% [34].

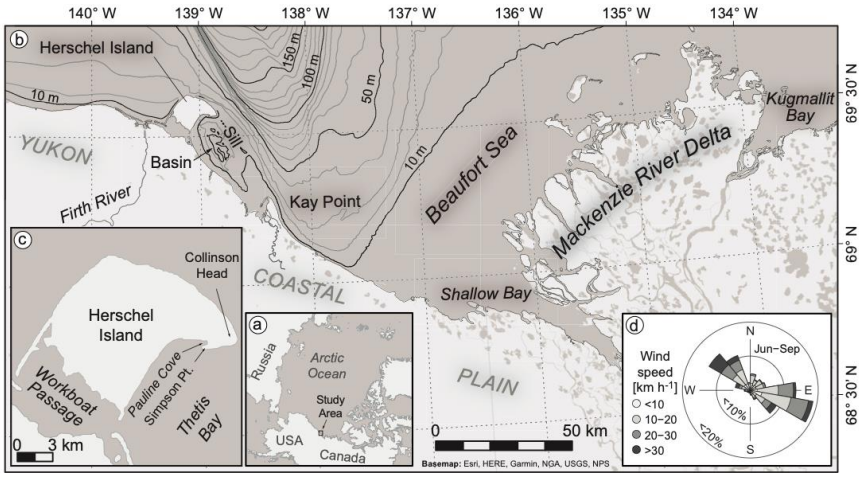

Figure 1. (**a**) The study area is located in the Canadian Beaufort Sea, (**b**) specifically in the vicinity of

Herschel Island—Qikiqtaruk with the Mackenzie River to the east, and the Firth River to the west. (**c**) The focus of the study lies on two localities: Thetis Bay and Workboat Passage. (**d**) Note the bimodal wind distribution during the 1995–2016 open water seasons recorded at Herschel Island—Qikiqtaruk [51–53].

2.1. Meteorological Conditions and Physical Processes

Open-water conditions typically occur from June to early October [54,55]. In the 1995–2016 open-water seasons, the wind distribution at HI was bimodal (Figure 1d). Prevailing SSE winds reached a maximum average hourly speed of 53 km h^{-1} (mean: 18.4, S.D.: 8.7) [53]. Dominant NW winds reached a maximum hourly speed of 84 km h^{-1} (mean: 21.7, S.D.: 12.4). NW winds set up longshore currents flowing eastward along the Yukon Coast and south along the island's western shore. East of the island, southeasterly winds generate westward longshore currents along the mainland coast, and westward- and southwestward flowing currents along the eastern shore of the island [56].

The astronomical tide range in the area is estimated at <0.4 m [57,58], however NW winds result in positive surges, while SSE winds produce negative ones [54,59]. Storm frequency is higher in late August and September. Most storms originate northwest of the island, and to a lesser extent in the south-southeast [60]. In the Beaufort Sea, fetch length may exceed 1000 km in September [61], allowing for wave heights exceeding 4 m, with wave periods up to 10 s [62].

Herschel Sill, a submerged shallow ridge, marks the extent of landfast ice during winter (Figure 1b), while a lead persists somewhat offshore of the sill where drifting pack ice moves clockwise to the west [57]. However, ice-related physical processes (e.g., ice scour, wallow pits, ice rafting, anchor ice, etc.) presumably affect the nearshore areas around HI [63] as winds can drive drifting ice into TB during the break-up period.

2.2. Coastal Geomorphology and Local Sediment Sources

The Mackenzie River dominates the entire Beaufort Shelf in terms of carbon and sediment input [2,37,38,64,65]. Depending on the season, the Mackenzie discharge ranges between 4000 to 23,000 m^3 s^{-1} [66]. The Mackenzie plume tends to drift eastward during the open water season whereas offshore water with significantly lower sediment concentrations is drawn southward past HI into Mackenzie Bay [56,57]. However, Mackenzie River sediments have been identified on inner shelf sediments of the Alaskan Beaufort Sea [39], ca. 400 km to the west of the study area.

Coastal bluffs (~25 m a.s.l.) comprise the dominant morphology of HI along TB. This section of HI is drained by several small streams. In addition, numerous retrogressive thaw slumps indicative of ice-rich permafrost are present. Coastal retreat rates in this part of the island range from 0–3.1 m a^{-1} [67], however rates up to 5.5 m a^{-1} have been reported [9]. Simpson Point (Figure 1c), a gravel spit located in the northeast of TB, also shelters the shoreline of Pauline Cove from waves (Section 2.1).

Workboat Passage (Figure 1c) is a shallow, fetch-limited lagoon enclosed by HI, its attached barriers, and the Yukon Coastal Plain. It is roughly 9 km long and ~5 km wide, and, except for the inlets, <2 m deep. In addition to two tidal inlets at each end of the lagoon, some portion of the Firth River reaches the lagoon in the west. The mean annual discharge of the river is 37.7 m^3 s^{-1} [68], while the mean discharge during freshet in June was 128.5 m^3 s^{-1} for the time period 1972–2014, according to a station maintained near the mouth by the Water Survey of Canada (http://wateroffice.ec.gc.ca/index_e.html, accessed: 15 April 2017). Low tundra and ice-poor cliffs (<6 m a.s.l.) characterize much of the Yukon mainland coast and the southeastern portion of HI, with shoreline retreat rates of 0.7 m a^{-1} along the Yukon Coast and 0.85 m a^{-1} along the eastern portion of HI, spanning the period between 1970–2011 in which the rate of coastal retreat significantly increased compared to the period of 1951–1970 [7,69].

3. Materials and Methods

Seabed samples were obtained using a Van Veen grab sampler during summer expeditions in 2012 and 2013. Sampling was performed along transects in water depths generally <13 m, to a distance of about 2 km offshore (5 km in WBP). Samples consisted of approximately 100 g of the top 3–6 cm of sediment and these samples were described on site. Samples were frozen a few hours after collection and freeze dried before sedimentological and geochemical analyses were carried out in the lab. Analytical and field data generated in this study are archived in a data repository [70]. Statistical differences among localities studied herein were tested using a two-tailed Wilcoxon-Mann–Whitney test ($\alpha = 0.01$). The statistical tools are published as a supplement in Radosavljevic [71]. The natural neighbor method was used for spatial interpolations.

3.1. Grain Size Analysis

Grain size distributions were obtained using laser diffractometry (LS200, Beckman Coulter, Brea, CA, USA). The <1 mm fraction of ca. 3 g of sample material with a dispersing agent (sodium hexaphosphate) was used for the measurements. Samples were previously oxidized with H_2O_2 to remove organics. Results are reported using graphical means following the method of Folk and Ward [72]. Grain size diameter is expressed in logarithmic phi (ϕ) units, where $\phi = -\log_2 D$, with D being the grain diameter in millimeters [73]. Phi values for grains coarser than one millimeter are negative, while those for grains finer than one millimeter are positive. The terminology for sorting and grainsize follows Blott and Pye [74].

3.2. Bulk Geochemical Analyses

The explanatory variables of particular interest reported in this study are the total organic carbon (TOC) content, the atomic organic carbon to total nitrogen (TN) ratio (hereafter referred to C/N ratio), and the stable carbon isotope signature ($\delta^{13}C$) of TOC. The C/N is an indicator of the source, nutritional value, and the degree of degradation of OM [75], although the actual reactivity and availability of TOC for microbial communities may be influenced by a fraction not detected by bulk measurements [31]. Clay-rich sediments, especially illite, adsorb ammonia [76]. The clay portion of sediments in the vicinity of HI contains 46–52% illite [43]. The correction for the adsorbed nitrogen requires subtracting the value of the intercept (given that a significant linear correlation of TOC and TN exists) [76]. In our case, the intercept was statistically indistinguishable from zero. Therefore, even though TN is not strictly organic bound, we assume the nitrogen in analyzed samples is predominantly free of clay-bound nitrogen and C/N ratios are representative of sedimentary OM.

The geochemical analyses share some preparatory steps such as freeze drying, homogenizing, and pulverizing a ca. 10 g subsample for eight minutes at 360 rpm inside a planetary mill (Fritsch, Idar-Oberstein, Germany, Pulverisette 5 classic line). Total carbon, TN, and TOC were determined using differential thermal analysis. Results of both analyses represent weight percent averages of aliquot pairs. Measurements were repeated if the results differed by more than 5%. Instrument calibration and performance monitoring was carried out using common standards. We computed C/N only where TOC and TN results fell above the detection limits (DL) for both elemental analyzers (0.1 wt.%). The analyses of TC, TIC, and TN do not constitute the focus of the current study and are presented in the Supplementary Materials.

The stable carbon isotope composition ($\delta^{13}C$) of OM is affected by its source material (terrestrial or marine derived OM). The $\delta^{13}C$ values were determined on carbonate-free samples (treated with 1.3 mol/L HCl) using isotope ratio mass spectrometers at the German Research Centre for Geosciences (GFZ) in Potsdam (DELTAplusXL, Thermo Fisher Scientific, Waltham, MA, USA) and at the University of Hamburg (Delta Vplus, Thermo Fisher Scientific, Waltham, MA, USA). Values are expressed in $\delta^{13}C$ per mille relative to VPDB (Vienna Pee Dee Belemnite).

3.3. Comparisons with Other Studies

We include comparisons to other studies which can be explored using the supplementary script [71]. Naidu et al. [38] provided data representative of marine samples. We selected samples with TOC, TN, and $\delta^{13}C$ values, at least 25 km offshore and less than 600 km off HI for this purpose. The spatial selection in Esri ArcMap was performed using a vector shoreline for the Beaufort Sea [52].

Terrestrial data was sourced from multiple studies. We subsampled the Couture et al. [34] dataset for Herschel Island samples, as the study included different landscape units along the Yukon Coast. Fritz et al. [47] sampled two permafrost exposures on the east side of the island. Tanski et al. [77] carried out a detailed sampling of a retrogressive thaw slump and the adjacent permafrost headwall and used a Normalized Difference Vegetation Index (NDVI) to classify the sampling locations based on vegetation and disturbance. Obu et al. [78] cored the active layer and the permafrost below on the east side of the island targeting landscape units derived from vegetation, some of which indicate disturbance. To compare these data with ours, we tagged sample data as disturbed, if the sediments were likely re-deposited on land, as indicated by the landscape unit classifications in the respective studies. Undisturbed samples contain permafrost and active layer samples from pristine Herschel Island landscapes. The terrestrial class in our comparison refers to the previously mentioned classes combined.

We compared bulk geochemical (TOC, TN, C/N, and $\delta^{13}C$) parameters of data gathered herein and auxiliary data using a bootstrap approach [79]. Means for each group were calculated with replacement using 50,000 iterations in R statistical environment [80]. The group means were compared using a Student's *t*-test.

4. Results

4.1. Granulometry

The 211 grain size distributions determined herein can be explored with the supplementary script [71]. Sediments are overall medium silt to very fine sand (mean: 5.2 ϕ, S.D.: 1.7) (Figure 2a) with moderate sorting (mean: 2.1 ϕ, S.D.: 0.5) (Figure 2b). Sediments in WBP are generally coarser than in TB (mean: 4.5 ϕ, S.D.: 1.1 and mean: 5.3 ϕ, S.D.: 1.7, respectively, *p*-value: 0.012) and show a distinctly different spatial distribution. In WBP, coarse and better sorted sandy sediments are found along the southeastern strike of the lagoon. The best sorted and coarsest sediments are located near the western tidal inlet. Finer, moderately to poorly sorted sediments are found closer to shore. The finest sediments are found in Pauline Cove, a small embayment in northern portion of TB. East of the spit, and in southern TB, sediments are progressively finer offshore. TB sediments are moderately sorted on average, with better sorting occurring close to shore. Sediments are poorly sorted beyond the 4 m contour. Cumulative frequency curves show a trend of increasing dominance of coarse sediments closer to shore, with largely fine samples offshore, and often exhibit multiple slope changes indicating different transport modes, which can be explored using the supplementary script [71].

4.2. Bulk Geochemical Data

4.2.1. Total Organic Carbon

The TOC content measured in our study range from <0.1 to 9.1 wt.%, with a mean of 1.0 wt.% (S.D.: 0.9). No significant difference between samples from WBP and TB was found (Supplementary Materials, Table S2), however, substantial differences exist spatially (Figure 3a). The highest values in WBP are found fringing the shores, while the lowest occupy the central portion of the lagoon. On the other hand, the highest values in TB are found in Pauline Cove, and immediately south of Simpson Point where samples contained coarse OM (e.g., wood fragments, peat). A sample in Pauline Cove consisting almost exclusively of woody fragments yielded the outlier of 9.1 wt.%. (next highest value of 3.8 wt.% is just south of Simpson Point). Total organic carbon comprises ~88% of the total carbon on average [71]. In order to remove outlier effects, we considered TOC data up to

the 95th percentile and found a significant correlation with a grain size of $\phi > 4$ ($R^2 = 0.57$, p-value: <0.001).

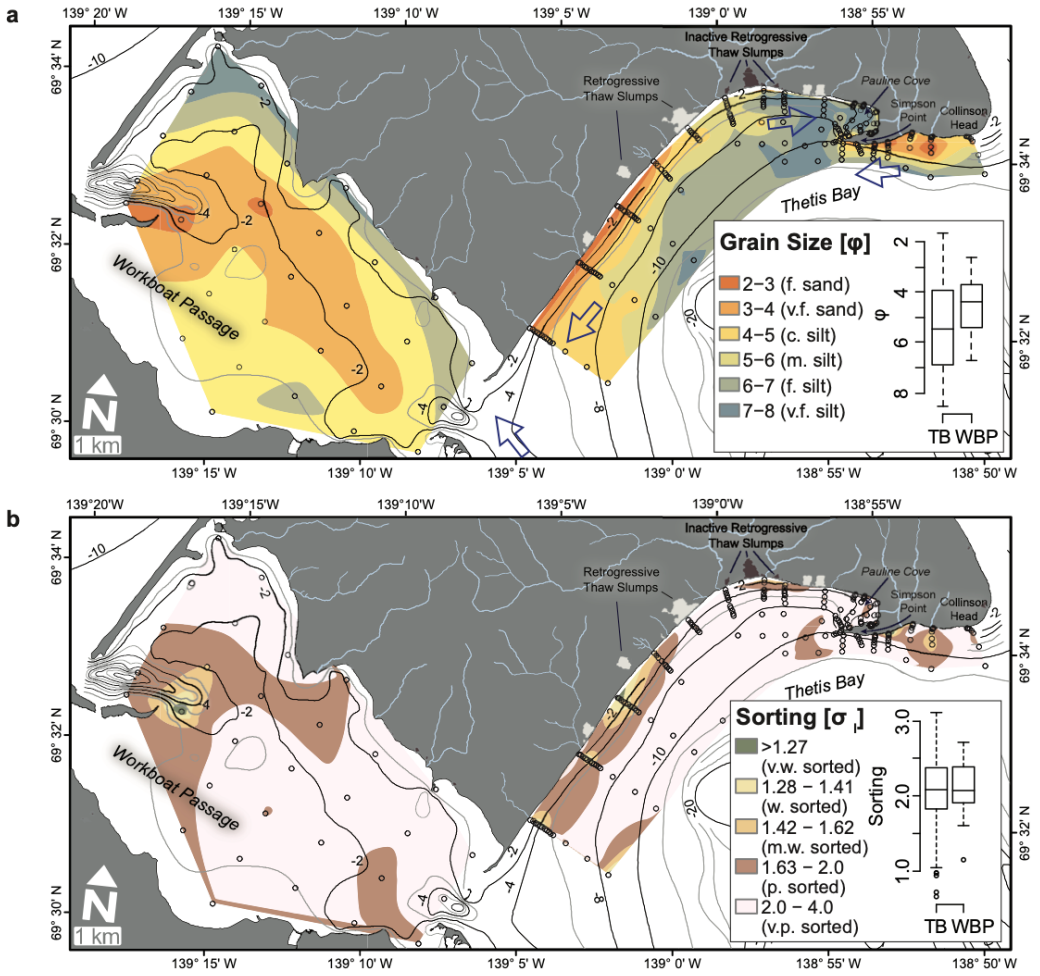

Figure 2. Spatial distribution and box plots of the (**a**) grain size mean and (**b**) sorting in the study area visualized using a natural neighbor interpolation and expressed in units of ϕ, where $\phi = -\log 2D$, with D being the grain diameter in millimeters. Size classes are indicated as fine (f.), medium (m.), and coarse (c.). Sorting is very well (v.w.), well (w.), moderately well (m.w.), poor (p.), and very poor (v.p.). Sample locations shown as open circles. Blue arrows indicate dominant longshore directions. Isobaths show 1 m contours in Workboat Passage (WBP), and 2 m contours in Thetis Bay (TB) [51,81,82].

4.2.2. Stable Carbon Isotopes and C/N Ratios

The contributions of terrestrial OM to nearshore sediments were assessed using stable carbon isotope analyses augmented by C/N. Stable carbon isotope analyses (n = 179) yielded a range of −27.4 to −25.3‰ (mean: −26.4, S.D.: 0.4‰), for samples in Pauline Cove and at Collinson Head (VF-02 and TB126001), respectively. There is a statistically significant difference between the $\delta^{13}C$ means in TB and WBP samples (Table S2). More $\delta^{13}C$-depleted values fringe the coast of WBP (Figure 3b). The samples obtained from these locations contained plant litter, while central, shallower areas with coarser sediments exhibit enriched $\delta^{13}C$ values and also contained living bivalves. In TB, depleted $\delta^{13}C$ values are just south of Simpson Point, along the southern coastline of TB, and in the vicinity of the massive retrogressive thaw slumps. These samples contained peat and wood fragments. More depleted $\delta^{13}C$ values were measured within Pauline Cove, to the SW of Simpson Point, and at the western end of the study area, where samples contained living benthic infauna (Polychaeta, bivalves).

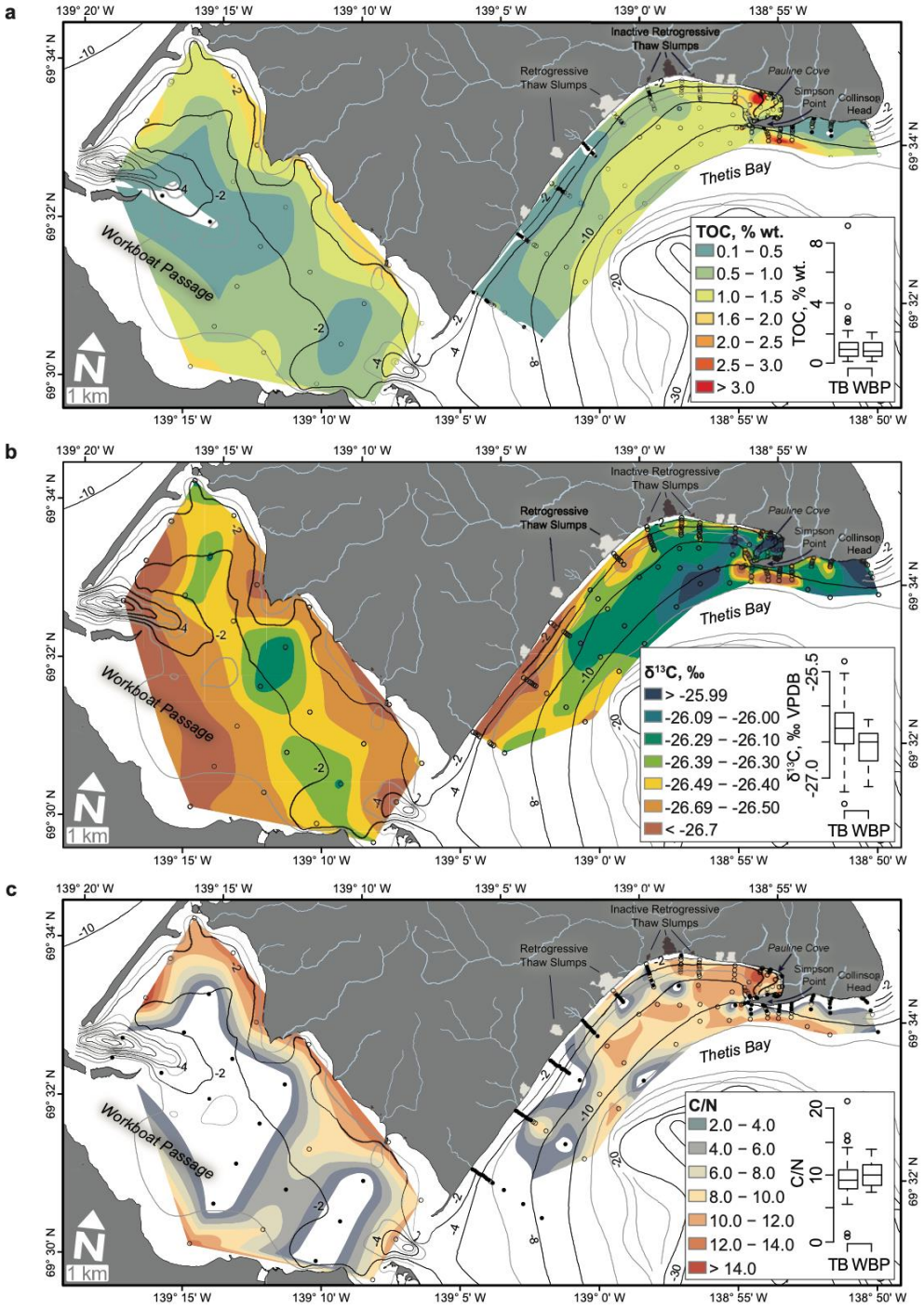

Figure 3. The spatial distribution and box plots of (**a**) total organic carbon content, (**b**) stable carbon isotopes ($\delta^{13}C$) and (**c**) carbon-nitrogen (C/N) ratio. Note higher $\delta^{13}C$ values in Pauline Cove and lower values along the fringes of WBP. Additionally, note high C/N in Pauline Cove and along the fringes of WBP. Locations of samples with either N or TOC below the detection limit are indicated by black solid circles and were not used in the interpolation. Isobaths show 1 m contours in WBP, and 2 m contours in TB [51,81,82].

Atomic C/N ratios were calculated for 99 samples. They are clustered around the mean (7.9, S.D.: 2.3) and no significant difference among TB and WBP was found (Figure 3c). In WBP, higher C/N values are located around the fringes of the lagoon, while in much of the lagoon center TOC and N measurements were below DL. In TB, the highest C/N

values were found within Pauline Cove, adjacent to a large thaw slump system (Figure S1), and seaward of the 8–10 m isobaths, but then only in the eastern part of TB. Statistical tests showed no correlation with grain size parameters.

4.3. Bootstrap Comparisons with Other Studies

Estimates of analyzed geochemical parameter population means using the bootstrap method are presented in Table 1 and Figure 4. Kernel density plots in Figure 4b show the distribution of means. The null hypothesis could be rejected in all pairwise comparisons of means of the current study with marine and terrestrial (disturbed, undisturbed as defined in the respective studies and combined) samples using a two-tailed Student's *t*-test.

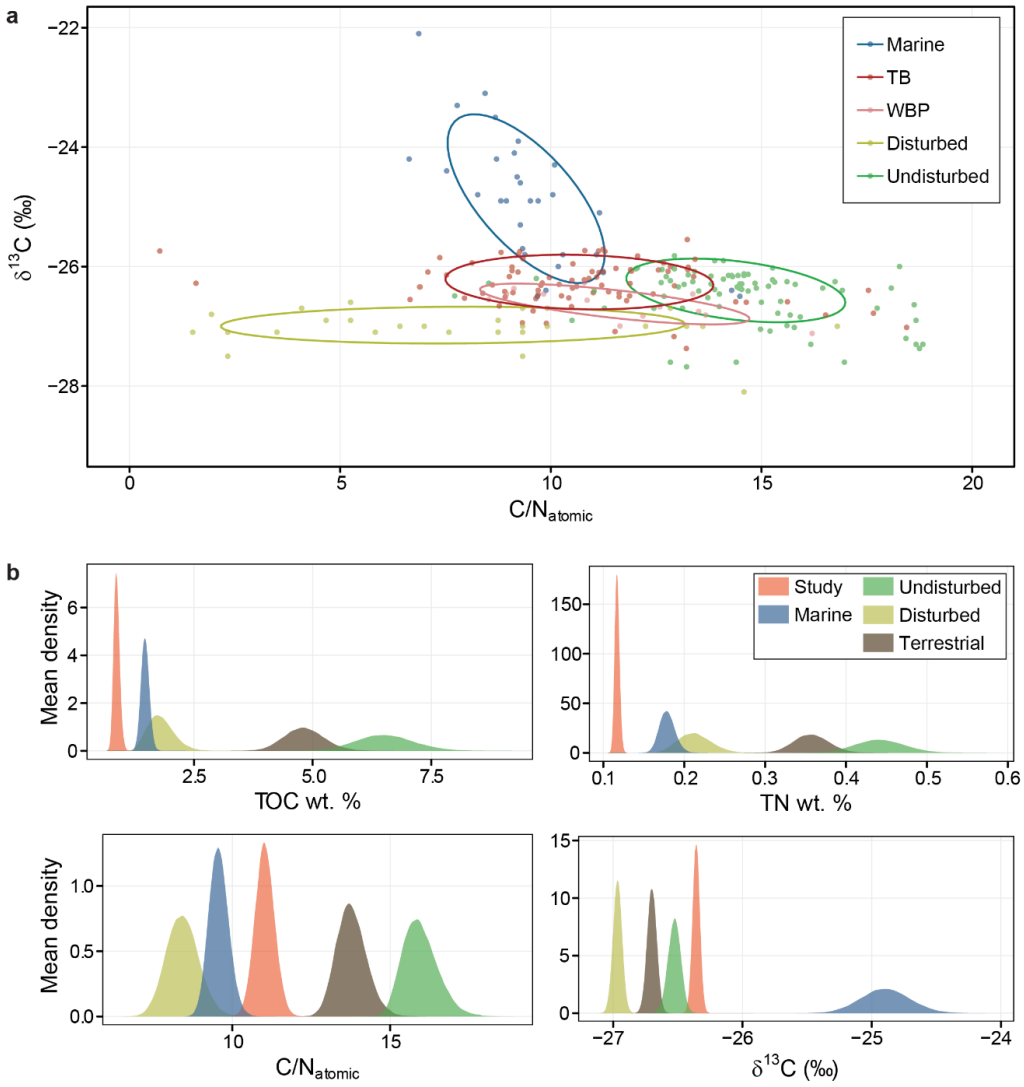

Figure 4. (**a**) Scatterplot showing the relation of stable carbon isotopes ($\delta^{13}C$) and atomic organic carbon-nitrogen (C/N) ratios along with concentration ellipses of one standard deviation, (**b**) bootstrap kernel density plot of parameter means. Shown are results of the current study localities of Thetis Bay and Workboat Passage (TB and WBP) and results from other studies in the region that focused on marine sediments (here 25 km offshore in the Beaufort Sea) (Naidu et al. [38], as well as sediments from disturbed and undisturbed landscapes on Herschel [34,77,78,83]. Disturbed and undisturbed sediments are combined under "terrestrial". $\delta^{13}C$ values are expressed as ‰ relative to the Vienna Pee Dee Belemnite (VPDB) standard.

Table 1. Estimations of population means and respective 0.01 and 0.99 percentiles (in parentheses) obtained through the bootstrap analysis. Terrestrial sample values were taken from other studies (see Section 3.3), including their classification into disturbed and undisturbed. We combined these for the overall terrestrial values.

	Sample Means (0.99 CI)			
	TOC [wt.%]	**TN [wt.%]**	**C/N [Atomic]**	**$\delta^{13}C$ [‰ VPDB]**
Study	0.87 (0.74, 1.02)	0.12 (0.11, 0.12)	11.03 (10.33, 11.75)	−26.36 (−26.42, −26.29)
Marine	1.47 (1.28, 1.67)	0.18 (0.16, 0.2)	9.57 (8.9, 10.33)	−24.89 (−25.33, −24.45)
Terrestrial (overall)	4.82 (3.9, 5.84)	0.36 (0.31, 0.41)	13.78 (12.78, 14.99)	−26.7 (−26.79, −26.62)
Terrestrial (Undisturbed)	6.53 (5.2, 8.01)	0.44 (0.37, 0.51)	15.95 (14.89, 17.41)	−26.53 (−26.64, −26.42)
Terrestrial (Disturbed)	1.8 (1.27, 2.53)	0.21 (0.17, 0.26)	8.43 (7.32, 9.68)	−26.97 (−27.05, −26.89)

5. Discussion

5.1. Sediment Dispersal, Accumulation and Redistribution

The two locations, WBP and TB differ in morphology, prevalence, and intensity of physical processes. Sediment grain size in TB has greater variance but is finer in comparison to WBP (Figure 2a), on average. Close to shore, along the eastern part and southwestern part of TB, well to moderately well-sorted, coarse skewed distributions of sand to very fine sand indicate relatively high hydrodynamic energy associated with waves and longshore currents which allow for winnowing of finer sediments. The persistence of hydrodynamically packed sandy sediments below the surface is corroborated by a geotechnical investigation carried out by Stark et al. [30]. This zone corresponds to the resuspension zone classified by an earlier study by Jong et al. 2020 [46]. Moderately- and poorly sorted muds ($\phi > 4$) are typically found beyond the 4 m contour (Figure 2b). This environment, ca. 100–300 m offshore, was described as the nearshore deposition zone [46], where a decline of surface water turbidity suggests deposition of suspended material [84]. Out of 116 samples seaward of the 4 m contour in TB, ca. 64% are very poorly sorted or poorly sorted. Rafting of coarser sediments by anchor ice, or bottom-fast ice may explain the poor sorting and is found along the Alaskan Beaufort Sea Coast [85], as well. From the south end of Thetis Bay, sediments become progressively finer toward Pauline Cove. Considering the prevailing SE winds and the morphology of barrier spits along TB, the longshore current direction is to the west and southwest [9,86]. Simpson Point, the spit on the western corner of HI, protects Pauline Cove and the area immediately west of the spit from wave attack allowing for fine silt deposition, presumably due to wave and current interaction with the rapid change in bathymetry.

Some of the poorest sorting found in this study is located in the bight of TB, south of three inactive slumps (Figure 2b). The area is subject to lower hydrodynamic energy given silty sediments found there, while multiple slope changes in cumulative grain size distribution curves (transects I-K in supplementary script) [71] indicate multiple transport processes. Considering the wind conditions during freeze-up and break-up, drifting patches of landfast ice may concentrate in the bight. Anchor ice and bottom-fast ice may be present to the 2 m contour, intense reworking by ice keel scour and ice rafting could be expected given the wind patterns. Keels of imbricated ice floes may possibly reach even greater depths. Corroborating data is not available, however the seabed backscatter imagery in this area was described as patchy, and penetrometer measurements indicate stiff sediments [30]. Intense ice scouring might expose the underlying substrate allowing little or no deposition here. Especially in TB, offshore transport is likely, given the low settling velocities of fine sediments. Herschel Basin sediments comprise 56 ± 6% of OC of sediments eroded from HI [87].

The sediment distribution pattern in WBP is controlled largely by the morphology and physical processes. Sediments enter the lagoon via longshore drift through two tidal inlets at opposite sides of the lagoon. Coastal retreat of 0.16 ± 0.35 m a^{-1} in WBP [69] contributes relatively little sediment to the lagoon. However, silty sediments along the northern fringe of the lagoon exhibiting enriched $\delta^{13}C$ and high C/N values could also be supplied by longshore currents, particularly under ESE wind conditions [84]. Fluvial input (i.e., Firth River) occurs ca. 3 km west of the study area. The mean annual flow for the Firth River is 37.7 m^3 s^{-1} [68]. The barrier island lagoon where the Firth River discharges is connected to WBP, therefore fluvial sediment input cannot be ruled out and may be indicated by enriched $\delta^{13}C$ values in the southwest of WBP. We interpret the shallow central portion of the lagoon as the flood tidal deposits reworked by waves and currents. The waves generated within the lagoon dissipate their energy on the shoal and fine sediments are winnowed. These may be deposited closer to the fringes of the lagoon (Figure 2a). The sediments in the center of the lagoon are fairly stiff and sandy indicating the persistent higher energy conditions and winnowing of low density and fine sediments, while sediments are soft along the western spit where deposition has been suggested [30]. Apart from the tidal inlets where sediments are moderately to well-sorted, sorting in the lagoon is poor, indicating the influence of ice-related processes or glacial source material.

In lower latitudes, sediment supply and hydrodynamic processes influence grain size distributions in nearshore sediments. Transport of grains occurs once wave- and tide-generated currents exceed the entrainment velocity for a given grain size. Once mobile, grains may be transported along the bottom or in suspension. However, unless the critical shear stress for all different sizes is exceeded, selective transport, i.e., winnowing occurs. Selective transport therefore sorts sediments. In our case, multiple physical processes are revealed by slope changes in the cumulative volumetric percentage curves [72,88]. These curves can be explored using the supplementary script [71]. In contrast to lower latitudes, ice processes in polar regions are able to entrain and transport sediments of various sizes (including OM) to deeper shelf areas. Super-cool water slush of frazil ice entrains predominantly fine grained sediments; while flotation of anchor ice incorporates sand- and gravel-sized material into sea ice [89]. Reimnitz et al. [28] documented a likelihood of ice-bonded sediment and anchor ice occurrence landward of the 20 m contour in the Alaskan Beaufort Sea. Grain size sorting can therefore indicate ice-related transport, as ice can transport and deposit coarser sediments where they would not occur given hydrodynamics alone.

The spatial variation of mean grain size reflects prevailing energy conditions within depositional environments. Our attempts to explain the variation using multiple linear models (combinations of depth, distance to coast, northing and easting) yielded adjusted coefficients of correlation of only 0.21–0.31 (not shown), indicating that higher order variables such as shoreline orientation, longshore transport and sediment supply might play a much more important role for the grain size distribution at any given point. However, we do observe a progressive decrease in grainsize offshore in TB. In the regional context, the Beaufort Sea shelf is characterized by clay size sediments [44].

The sediments analyzed herein are mostly fine-grained and have low settling velocities. Although the sediments examined in the following comparison were slightly sandier than in the current study, bed failure occurs with critical shear velocities of 1.3–1.7 cm s^{-1}, while resuspension of the less consolidated upper layer occurs at velocities 1.1–1.3 cm s^{-1} [29]. Lintern et al. [27] observed current velocities of 2–25 cm s^{-1}, ca. 120 km east of Herschel Island, during a quiescent period using a current meter mounted 0.5 m above the bed in 7 m depth, but during storm events, sediments similar to the ones in the current study are easily entrained. Therefore, we can assume that the sediments in the study area are frequently resuspended and that at least a portion of sediments is exported beyond the current study extent.

5.2. Total Organic Carbon Content

The TOC concentrations in the studied sediments are similar to sediments elsewhere in the Arctic Ocean [39,90,91] and fit into the general OC distribution pattern on the Beaufort Shelf [44,92]. OC concentrations in sediments of the Arctic Ocean range 0–16.5 wt.%, ranging 0.55–1.45 wt.% between the 75th and 25th percentiles [92], therefore our results are representative of the Arctic Basin and are comparable to values found in lower latitudes [93]. We found a correlation of TOC with muddy sediments (silt and clay fraction), as greater mineral surface area also aids sorption of OM [94,95]. Processes responsible for transport and sorting of sediments also influence the distribution of OC [39,96]. Coarser OM typically constitutes a minor fraction in the marine environment and is retained closer to shore where physical reworking aids in disaggregation [97]. Considering both study area locations, elevated TOC values were found in areas of lower hydrodynamic energy, such as the fringe of WBP, Pauline Cove, and seaward of the 8 m isobaths in TB (Figure 3a). In the shallow WBP, physical reworking is more intense and while there is less variance of TOC values, no significant difference was found in comparison to TB (Figure 3a, Table S2).

We compared the results herein with published TOC measurements from sediments on HI and the Yukon mainland and marine sediments in the Beaufort Sea (Tables 1 and S1). Terrestrial permafrost sediments were furthermore classified as undisturbed if they originated from the active layer and the permafrost below, or disturbed if the re-deposited permafrost sediments were sampled. Several comparisons were made and can also be explored using the supplementary script [71]. Our comparisons established significant statistical differences in pairwise comparisons of TOC means using sample means and bootstrap estimates. Terrestrial sediments contain approximately five times more TOC than nearshore sediments by weight (Table 1) using the population mean estimates. Furthermore, the bootstrap estimates are on the same order of magnitude as previous studies on Herschel Island which report an average of 3.17 wt.% TOC [47] (this dataset was included in the bootstrap) or 1.4–4.4 wt.% TOC [98].

The partial TOC transfer to other pools (e.g., dissolved organic carbon, atmosphere, and shelf sediments) is related to physical and biochemical processes, and explains the difference in concentration of TOC in marine and terrestrial sediments. Terrestrial permafrost OM is vulnerable to continued warming [99] and is reactive, as demonstrated by field and laboratory experiments [100–102], although only a fraction is readily decomposed over short time scales (e.g., <5%), and 20–90% could be mineralized over a 50 year incubation period [103]. Tanski et al. [77] investigated changes of bulk sediment geochemical properties including OC within a retrogressive thaw slump floor on HI (Figure S1). The results showed that disturbed sediments on the slump floor contained ca. 80% less TOC on average compared to undisturbed sediments. According to Tanski et al. [77], OC is rapidly leached and mineralized from particulate OM [104]. Leaching of OC into the dissolved phase likely also applies in our case [105,106], as sea water is an efficient leaching agent [107]. The dataset presented in this study has a greater spatial coverage and resolution than Tanski et al. [77], yet we confirmed (not shown) that disturbed sediment OM from mud pools in the retrogressive thaw slump is statistically indistinguishable from nearshore sediments (p-value: <0.001), as stated by Tanski et al. [77]. Therefore, disturbances of permafrost cause rapid OC loss and it is likely that OC is further mineralized in the nearshore where a range of physical and geochemical processes operate. With the current methodology, it cannot be ascertained to what extent degradation processes such as priming, photooxidation [26], physical breakdown, or the fungal mineralization of refractory OM [25] affect nearshore TOC content. Fluid mud layers are present in the study area [30] which indicates that the nearshore area of HI is a dynamic environment with a high potential for resuspension and OM degradation [24], but also for offshore transport. The latter is corroborated by the spatial pattern of TOC and its correlation with fine sediments which are easily transported beyond the study area, as stated previously. Other studies utilized stable and radiocarbon isotopes, neodymium isotopes, nitrogen isotopes algal pigments, and lignin-phenols to constrain the contributions of the refractory pool [39,41,108].

5.3. Nearshore Organic Matter Characteristics

To decrease the sensitivity of statistical tests to outliers, we compared TOC, N and C/N using a bootstrap approach. Apart from $\delta^{13}C$, significant differences were found among the parameter means for nearshore samples of this study, terrestrial (both disturbed and undisturbed) and marine samples (Figure 4, Tables 1 and S1). The $\delta^{13}C$ distribution illustrates that nearshore areas represent the transition between terrestrial and marine sediments (Figure 4a). Disturbed sediments exhibit the most depleted $\delta^{13}C$ values as this material enriched by OM of colonizing plants. Terrestrial samples with depleted $\delta^{13}C$ and high C/N are most similar to sediments from WBP (Figures 3 and 4a). The lagoon (WBP) receives eroded shore sediments from HI and the Yukon mainland, longshore transport from both the northwest and northeast [86], but also a portion of the Firth River discharge. The regions closer to shore also exhibit higher C/N values pointing to less degraded OM that is likely of terrestrial origin. It is likely that OM degradation starts on land once permafrost thaws and landscape disturbance occurs, indicated by significantly lower TOC and TN concentrations in nearshore environments compared to terrestrial samples (Figure 4b). This confirms the findings of an earlier study across the different ecological and morphological zones in a retrogressive thaw slump [77].

However, the distribution of these values is also heavily influenced by physical processes as explained in Section 5.1. The central portion of the lagoon contains sandy sediments where some carbon and nitrogen contents were below the instrument detection limit. Similar sediments are also found in the southwestern and eastern portion of TB. Sediments in TB are enriched in marine carbon as indicated by $\delta^{13}C$ and include a wider range of C/N values, locally influenced by thermokarst processes (thaw slumps).

An interesting case is Pauline Cove, the small embayment in northeastern TB. High values of C/N indicate that OM is less degraded. However, enriched $\delta^{13}C$ values suggest a greater marine influence. We attribute this to the sheltering effect of Simpson Point that allows terrestrial OM to accumulate, but the sheltering also augments primary production in the less turbid water column. This could partly explain enriched $\delta^{13}C$, and in addition, our sampling also collected tubeworms (~5–15% of sample) along with the sediment. Stable carbon isotopes of tubeworms [20] are higher than terrestrial OM derived from plants utilizing the C3 pathway common in the Arctic [109].

Previous studies used $\delta^{13}C$ signatures to estimate the relative percentages of terrigenous and marine organic carbon in analyzed samples using a two end member model [34,109,110]. A significant portion of HI sediments originated from Herschel Basin by glacial ice thrust during the late Pleistocene and is of marine origin [49,50,111]. Although the bootstrapped *t*-test comparison of means for undisturbed terrestrial and nearshore sediment was significant (*p*-value: <0.001), the ca. 0.2‰ difference in means for these two groups underscores the marine origin of HI. Furthermore, the limited applicability of stable isotope mixing models in polar regions has been noted previously [112]. Two end-member mixing models incorporate bulk OC, and are very sensitive to end-member values [109]. Other approaches, such as chemical biomarker and molecular signature analyses, could provide a better answer on the contributions of terrestrial carbon in the nearshore [33,39,87]. The separation of the carbon pool into its refractory and labile components could also be addressed by incorporating nitrogen isotopes in the end member model [107], while permafrost carbon contributions can be addressed by radiocarbon dating [87].

An important question is if the nearshore zone can sequester terrestrial carbon. This depends on the burial efficiency, the ratio of OM burial rate and the OM input rate, where burial refers to sediments buried below the oxic layer. Therefore, if OM were to be sequestered, the supply rate needs to exceed the burial rate [94,113]. Arctic nearshore areas are thought to be dominated by erosion [54] when taking into account the physical processes in the nearshore described in Section 5.1. Nevertheless, the nearshore deposition zone apparently functions as a sediment sink, at least temporarily [46]. Unlithified permafrost coasts represent 65% of the total shoreline in the Arctic [10]. Results from the Laptev and the Beaufort seas show that a large percentage of carbon contained in sediments of the inner

shelf originates from erosion of the shelf itself [39,41], and is further deposited on the outer shelf [1]. The changing physical conditions are expected to increase shoreline retreat [4], which will be accompanied by shoreface erosion as well. However, barrier islands and spits provide shelter for lagoons and embayments, where the sediment accumulation rate could facilitate carbon burial. Settings such as the fringe of WBP and Pauline Cove in TB may function as carbon sinks [56]. Perhaps similar settings along the Yukon Coast (e.g., Ptarmigan Bay, Phillips Bay, Roland Bay, etc.) function as sediment traps. In the deep Herschel Basin just SE of the current study area, more than 12 m of sediments have accumulated over the last ~4000 years and ca. 56% originate from coastal erosion of Herschel Island [87]. Future studies should attempt to quantify sedimentation rates in these settings, a prerequisite for a carbon budget.

6. Conclusions

Using grain size data and various bulk geochemical indicators, we determined the patterns of sediment transport and OM distribution in an Arctic nearshore setting along erosive permafrost coasts near Herschel Island in the western Canadian Arctic. Further, we deciphered the main processes controlling the fate of OM in the region. The spatial distribution of sediments in the study area is indicative of the predominance of hydrodynamic processes, mostly related to waves and longshore currents. Ice rafting of sediments is also apparent by observations of moderately to poorly sorted sediments seaward of the 2 m contour. A significant correlation of TOC (mean: 1.02 wt.%) was found with mud content, thus suggesting that geochemical parameters generally follow spatial trends in grain size. Apart from this correlation, our fitted models could not explain the parameters indicating that higher order variables (shoreline orientation, longshore transport, sediment supply) play a much more important role for the grain size distribution at any given point.

Nearshore sediments contain ~4–5 times less TOC than terrestrial sediments in the study area. In comparison to terrestrial sediments, lower C/N values in the nearshore suggest degradation and hint at the redistribution of permafrost OM on the arctic nearshore. The association of TOC with fine grain size fractions and easy resuspension also indicates a significant portion of TOC may be exported beyond the study area. Our results show that the arctic shoreface of the Yukon coast is comparable to other coastal sections of the Beaufort Sea.

Supplementary Materials: The following supporting information can be downloaded at: https://www.mdpi.com/article/10.3390/jmse10111589/s1. Reference [114] is cited in the Supplementary Materials.

Author Contributions: Conceptualization, B.R. and H.L.; methodology, B.R. and H.L.; investigation, B.R. and C.K., formal analysis, B.R. and U.H.; data curation, B.R.; writing—original draft preparation, B.R.; writing—review and editing, M.F., H.L., C.K., N.C. and U.H.; visualization, B.R.; project administration, H.L.; funding acquisition, H.L. and M.F. All authors have read and agreed to the published version of the manuscript.

Funding: This work was funded by the Helmholtz Association (grant no. VH-NG-801 to H.L.). The work of M.F. was supported by the Daimler and Benz Foundation (grant no. 32-02/15). C.K. was funded by the Cluster of Excellence 'CliSAP' (EXC177), Universität Hamburg. We are grateful to Yukon Territorial Government, Yukon Parks (Herschel Island Quiqiktaruk Territorial Park) and the Aurora Research Institute.

Institutional Review Board Statement: Not applicable.

Informed Consent Statement: Not applicable.

Data Availability Statement: Data used in this study has been archived in an open access repository and is cited in the text as Radosavljevic, B., H. Lantuit, B. Plessen, and C. Knoblauch. 2016. Granulometry and bulk geochemistry of nearshore sediments, Herschel Island, Yukon Territory, Canada. PANGAEA. https://doi.org/10.1594/PANGAEA.859116. The supplementary script is cited in the text as Radosavljevic, B. Tools for Statistical Evaluation and Exploration of Granulometric and Bulk Geochemical Data; GFZ Data Services: Potsdam, Germany, 2018. https://doi.org/10.5880/GFZ.LIS.2018.001.

Acknowledgments: We would like to thank Birgit Plessen, Hanno Meyer, Maximilian Frick, Elisabeth Schönfeldt, Mario Reichenbach, Ute Kuschel, George Tanski, Stefanie Weege, and Juliane Wolter for help with field- and lab work, and Marko Abramović for final figure editing. This is Natural Resources Canada contribution number 20220373 (Canadian Crown copyright reserved). We acknowledge support by the Open Access Publication Funds of Alfred-Wegener-Institut Helmholtz-Zentrum für Polar- und Meeresforschung.

Conflicts of Interest: The authors declare no conflict of interest.

References

1. Wegner, C.; Bennett, K.E.; de Vernal, A.; Forwick, M.; Fritz, M.; Heikkilä, M.; Łącka, M.; Lantuit, H.; Laska, M.; Moskalik, M.; et al. Variability in Transport of Terrigenous Material on the Shelves and the Deep Arctic Ocean during the Holocene. *Polar Res.* **2015**, *34*, 24964. [CrossRef]
2. Rachold, V.; Eicken, H.; Gordeev, V.V.; Grigoriev, M.N.; Hubberten, H.-W.; Lisitzin, A.P.; Shevchenko, V.P.; Schirrmeister, L. Modern Terrigenous Organic Carbon Input to the Arctic Ocean. In *The Organic Carbon Cycle in the Arctic Ocean*; Stein, R., Macdonald, R.W., Eds.; Springer: Berlin/Heidelberg, Germany, 2004; pp. 33–55. ISBN 978-3-642-18912-8.
3. Barnhart, K.R.; Overeem, I.; Anderson, R.S. The Effect of Changing Sea Ice on the Vulnerability of Arctic Coasts. *Cryosphere* **2014**, *8*, 1777–1799. [CrossRef]
4. Manson, G.K.; Solomon, S.M. Past and Future Forcing of Beaufort Sea Coastal Change. *Atmosphere-Ocean* **2007**, *45*, 107–122. [CrossRef]
5. Overeem, I.; Anderson, R.S.; Wobus, C.W.; Clow, G.D.; Urban, F.E.; Matell, N. Sea Ice Loss Enhances Wave Action at the Arctic Coast. *Geophys. Res. Lett.* **2011**, *38*, L17503. [CrossRef]
6. Günther, F.; Overduin, P.P.; Baranskaya, A.; Opel, T.; Grigoriev, M.N. Observing Muostakh Island Disappear: Erosion of a Ground-Ice-Rich Coast in Response to Summer Warming and Sea Ice Reduction on the East Siberian Shelf. *Cryosphere* **2015**, *9*, 151–178. [CrossRef]
7. Irrgang, A.M.; Hugues, L.; Manson, G.K.; Frank, G.; Guido, G.; Overduin, P.P. Variability in Rates of Coastal Change Along the Yukon Coast, 1951 to 2015. *J. Geophys. Res. Earth Surf.* **2018**, *123*, 779–800. [CrossRef]
8. Jones, B.M.; Arp, C.D.; Jorgenson, M.T.; Hinkel, K.M.; Schmutz, J.A.; Flint, P.L. Increase in the Rate and Uniformity of Coastline Erosion in Arctic Alaska. *Geophys. Res. Lett.* **2009**, *36*, 1–5. [CrossRef]
9. Radosavljevic, B.; Lantuit, H.; Pollard, W.; Overduin, P.; Couture, N.; Sachs, T.; Helm, V.; Fritz, M. Erosion and Flooding—Threats to Coastal Infrastructure in the Arctic: A Case Study from Herschel Island, Yukon Territory, Canada. *Estuaries Coasts* **2015**, *39*, 900–915. [CrossRef]
10. Lantuit, H.; Overduin, P.P.; Couture, N.; Wetterich, S.; Aré, F.; Atkinson, D.; Brown, J.; Cherkashov, G.; Drozdov, D.; Forbes, D.L. The Arctic Coastal Dynamics Database: A New Classification Scheme and Statistics on Arctic Permafrost Coastlines. *Estuaries Coasts* **2012**, *35*, 383–400. [CrossRef]
11. Jorgenson, M.T.; Brown, J. Classification of the Alaskan Beaufort Sea Coast and Estimation of Carbon and Sediment Inputs from Coastal Erosion. *Geo-Mar. Lett.* **2005**, *25*, 69–80. [CrossRef]
12. Knoblauch, C.; Beer, C.; Sosnin, A.; Wagner, D.; Pfeiffer, E.-M. Predicting Long-Term Carbon Mineralization and Trace Gas Production from Thawing Permafrost of Northeast Siberia. *Glob. Change Biol.* **2013**, *19*, 1160–1172. [CrossRef] [PubMed]
13. Koven, C.D.; Schuur, E.A.G.; Schädel, C.; Bohn, T.J.; Burke, E.J.; Chen, G.; Chen, X.; Ciais, P.; Grosse, G.; Harden, J.W.; et al. A Simplified, Data-Constrained Approach to Estimate the Permafrost Carbon–Climate Feedback. *Philos. Trans. R. Soc. Lond. Math. Phys. Eng. Sci.* **2015**, *373*, 20140423. [CrossRef] [PubMed]
14. Macdonald, R.W.; Kuzyk, Z.Z.A.; Johannessen, S.C. The Vulnerability of Arctic Shelf Sediments to Climate Change. *Environ. Rev.* **2015**, *23*, 461–479. [CrossRef]
15. Opsahl, S.; Benner, R.; Amon, R.M.W. Major Flux of Terrigenous Dissolved Organic Matter through the Arctic Ocean. *Limnol. Oceanogr.* **1999**, *44*, 2017–2023. [CrossRef]
16. Rachold, V.; Grigoriev, M.N.; Are, F.E.; Solomon, S.; Reimnitz, E.; Kassens, H.; Antonow, M. Coastal Erosion vs. Riverine Sediment Discharge in the Arctic Shelf Seas. *Int. J. Earth Sci.* **2000**, *89*, 450–460. [CrossRef]
17. Schuur, E.A.G.; Abbott, B.W.; Bowden, W.B.; Brovkin, V.; Camill, P.; Canadell, J.G.; Chanton, J.P.; Chapin, F.S.; Christensen, T.R.; Ciais, P.; et al. Expert Assessment of Vulnerability of Permafrost Carbon to Climate Change. *Clim. Chang.* **2013**, *119*, 359–374. [CrossRef]
18. Ramage, J.L.; Irrgang, A.M.; Morgenstern, A.; Lantuit, H. Increasing Coastal Slump Activity Impacts the Release of Sediment and Organic Carbon into the Arctic Ocean. *Biogeosciences* **2018**, *15*, 1483–1495. [CrossRef]
19. Fritz, M.; Vonk, J.E.; Lantuit, H. Collapsing Arctic Coastlines. *Nat. Clim. Chang.* **2017**, *7*, 6. [CrossRef]
20. Dunton, K.H.; Weingartner, T.; Carmack, E.C. The Nearshore Western Beaufort Sea Ecosystem: Circulation and Importance of Terrestrial Carbon in Arctic Coastal Food Webs. *Prog. Oceanogr.* **2006**, *71*, 362–378. [CrossRef]
21. Hill, P.R.; Nadeau, O.C. Storm-Dominated Sedimentation on the Inner Shelf of the Canadian Beaufort Sea. *J. Sediment. Res.* **1989**, *59*, 455–468. [CrossRef]

22. Retamal, L.; Bonilla, S.; Vincent, W.F. Optical Gradients and Phytoplankton Production in the Mackenzie River and the Coastal Beaufort Sea. *Polar Biol.* **2007**, *31*, 363–379. [CrossRef]
23. Laruelle, G.G.; Dürr, H.H.; Lauerwald, R.; Hartmann, J.; Slomp, C.P.; Goossens, N.; Regnier, P.A.G. Global Multi-Scale Segmentation of Continental and Coastal Waters from the Watersheds to the Continental Margins. *Hydrol. Earth Syst. Sci.* **2013**, *17*, 2029–2051. [CrossRef]
24. Blair, N.E.; Aller, R.C. The Fate of Terrestrial Organic Carbon in the Marine Environment. *Annu. Rev. Mar. Sci.* **2012**, *4*, 401–423. [CrossRef] [PubMed]
25. Hyde, K.D.; Jones, E.B.G.; Leaño, E.; Pointing, S.B.; Poonyth, A.D.; Vrijmoed, L.L.P. Role of Fungi in Marine Ecosystems. *Biodivers. Conserv.* **1998**, *7*, 1147–1161. [CrossRef]
26. Estapa, M.L.; Mayer, L.M. Photooxidation of Particulate Organic Matter, Carbon/Oxygen Stoichiometry, and Related Photoreactions. *Mar. Chem.* **2010**, *122*, 138–147. [CrossRef]
27. Lintern, D.G.; Macdonald, R.W.; Solomon, S.M.; Jakes, H. Beaufort Sea Storm and Resuspension Modeling. *J. Mar. Syst.* **2013**, *127*, 14–25. [CrossRef]
28. Reimnitz, E.; Kempema, E.W.; Barnes, P.W. Anchor Ice, Seabed Freezing, and Sediment Dynamics in Shallow Arctic Seas. *J. Geophys. Res.* **1987**, *92*, 14671–14678. [CrossRef]
29. Walker, T.R.; Grant, J.; Cranford, P.; Lintern, D.G.; Hill, P.; Jarvis, P.; Barrell, J.; Nozais, C. Suspended Sediment and Erosion Dynamics in Kugmallit Bay and Beaufort Sea during Ice-Free Conditions. *J. Mar. Syst.* **2008**, *74*, 794–809. [CrossRef]
30. Stark, N.; Radosavljevic, B.; Quinn, B.; Lantuit, H. Application of Portable Free-Fall Penetrometer for Geotechnical Investigation of Arctic Nearshore Zone. *Can. Geotech. J.* **2016**, *54*, 31–46. [CrossRef]
31. Bianchi, T.S. The Role of Terrestrially Derived Organic Carbon in the Coastal Ocean: A Changing Paradigm and the Priming Effect. *Proc. Natl. Acad. Sci. USA* **2011**, *108*, 19473–19481. [CrossRef]
32. Belicka, L.L.; Macdonald, R.W.; Harvey, H.R. Sources and Transport of Organic Carbon to Shelf, Slope, and Basin Surface Sediments of the Arctic Ocean. *Deep Sea Res. Part Oceanogr. Res. Pap.* **2002**, *49*, 1463–1483. [CrossRef]
33. Bröder, L.; Tesi, T.; Andersson, A.; Eglinton, T.I.; Semiletov, I.P.; Dudarev, O.V.; Roos, P.; Gustafsson, Ö. Historical Records of Organic Matter Supply and Degradation Status in the East Siberian Sea. *Org. Geochem.* **2016**, *91*, 16–30. [CrossRef]
34. Couture, N.J.; Irrgang, A.; Pollard, W.; Lantuit, H.; Fritz, M. Coastal Erosion of Permafrost Soils Along the Yukon Coastal Plain and Fluxes of Organic Carbon to the Canadian Beaufort Sea. *J. Geophys. Res. Biogeosci.* **2018**, *123*, 406–422. [CrossRef]
35. Goñi, M.A.; Yunker, M.B.; Macdonald, R.W.; Eglinton, T.I. Distribution and Sources of Organic Biomarkers in Arctic Sediments from the Mackenzie River and Beaufort Shelf. *Mar. Chem.* **2000**, *71*, 23–51. [CrossRef]
36. Goñi, M.A.; Yunker, M.B.; Macdonald, R.W.; Eglinton, T.I. The Supply and Preservation of Ancient and Modern Components of Organic Carbon in the Canadian Beaufort Shelf of the Arctic Ocean. *Mar. Chem.* **2005**, *93*, 53–73. [CrossRef]
37. Macdonald, R.W.; Naidu, A.S.; Yunker, M.B.; Gobeil, C. The Beaufort Sea: Distribution, Sources, Fluxes and Burial of Organic Carbon. In *The Organic Carbon Cycle in the Arctic Ocean*; Stein, R., Macdonald, R.W., Eds.; Springer Publishing Company: Berlin, Germany, 2004; pp. 177–193.
38. Naidu, A.S.; Cooper, L.W.; Finney, B.P.; Macdonald, R.W.; Alexander, C.; Semiletov, I.P. Organic Carbon Isotope Ratios (Δ13C) of Arctic Amerasian Continental Shelf Sediments. *Int. J. Earth Sci.* **2000**, *89*, 522–532. [CrossRef]
39. Schreiner, K.M.; Bianchi, T.S.; Eglinton, T.I.; Allison, M.A.; Hanna, A.J.M. Sources of Terrigenous Inputs to Surface Sediments of the Colville River Delta and Simpson's Lagoon, Beaufort Sea, Alaska: Inputs to the colville river delta, AK. *J. Geophys. Res. Biogeosciences* **2013**, *118*, 808–824. [CrossRef]
40. Schubert, C.J.; Stein, R. Deposition of Organic Carbon in Arctic Ocean Sediments: Terrigenous Supply vs. Marine Productivity. *Org. Geochem.* **1996**, *24*, 421–436. [CrossRef]
41. Vonk, J.E.; Sánchez-García, L.; van Dongen, B.E.; Alling, V.; Kosmach, D.; Charkin, A.; Semiletov, I.P.; Dudarev, O.V.; Shakhova, N.; Roos, P.; et al. Activation of Old Carbon by Erosion of Coastal and Subsea Permafrost in Arctic Siberia. *Nature* **2012**, *489*, 137–140. [CrossRef]
42. Schreiner, K.M.; Bianchi, T.S.; Rosenheim, B.E. Evidence for Permafrost Thaw and Transport from an Alaskan North Slope Watershed. *Geophys. Res. Lett.* **2013**, *41*, 3117–3126. [CrossRef]
43. Pelletier, B.R. *Sediment Dispersal in the Southern Beaufort Sea*; Beaufort Sea Project, Department of the Environment, Natural Resources Canada: Victoria, BC, Canada, 1975.
44. *Marine Science Atlas of the Beaufort Sea: Sediments/Atlas Des Sciences Marines de La Mer de Beaufort: Sédiments*; Minister of Supply and Services: Ottawa, ON, Canada, 1984; ISBN 0-660-52681-6.
45. Jerosch, K. Geostatistical Mapping and Spatial Variability of Surficial Sediment Types on the Beaufort Shelf Based on Grain Size Data. *J. Mar. Syst.* **2013**, *127*, 5–13. [CrossRef]
46. Jong, D.; Bröder, L.; Tanski, G.; Fritz, M.; Lantuit, H.; Tesi, T.; Haghipour, N.; Eglinton, T.I.; Vonk, J.E. Nearshore Zone Dynamics Determine Pathway of Organic Carbon from Eroding Permafrost Coasts. *Geophys. Res. Lett.* **2020**, *47*, e2020GL088561. [CrossRef] [PubMed]
47. Fritz, M.; Wetterich, S.; Schirrmeister, L.; Meyer, H.; Lantuit, H.; Preusser, F.; Pollard, W.H. Eastern Beringia and beyond: Late Wisconsinan and Holocene Landscape Dynamics along the Yukon Coastal Plain, Canada. *Palaeogeogr. Palaeoclimatol. Palaeoecol.* **2012**, *319–320*, 28–45. [CrossRef]
48. Mackay, J.R. Glacier Ice-Thrust Features of the Yukon Coast. *Geogr. Bull.* **1959**, *13*, 5–21.

49. Rampton, V.N. *Quaternary Geology of the Yukon Coastal Plain*; Geological Survey of Canada: Ottawa, ON, Canada, 1982; ISBN 0-660-10637-X.
50. Pollard, W.H. The Nature and Origin of Ground Ice in the Herschel Island Area, Yukon Territory. In Proceedings of the Fifth Canadian Permafrost Conference, Quebec, QC, Canada, 6–8 June 1990; pp. 23–30.
51. Thompson, F. *Illustrations from: An Interpretive Manual for Reports on Granular Deposits in the Inuvialuit Settlement Region: Part of the Inuvialuit Final Agreement Implementation Program, Task 7-Sand and Gravel*; Indian and Northern Affairs Canada; Northern Affairs Program: Ottawa, ON, Canada, 1994; p. 53.
52. Wessel, P.; Smith, W.H.F. A Global, Self-Consistent, Hierarchical, High-Resolution Shoreline Database. *J. Geophys. Res. Solid Earth* **1996**, *101*, 8741–8743. [CrossRef]
53. Environment and Climate Change Canada Historical Data-Climate-Environment and Climate Change Canada. Available online: http://climate.weather.gc.ca/historical_data/search_historic_data_e.html (accessed on 24 April 2017).
54. Héquette, A.; Barnes, P.W. Coastal Retreat and Shoreface Profile Variations in the Canadian Beaufort Sea. *Mar. Geol.* **1990**, *91*, 113–132. [CrossRef]
55. Solomon, S.M. Spatial and Temporal Variability of Shoreline Change in the Beaufort-Mackenzie Region, Northwest Territories, Canada. *Geo-Mar. Lett.* **2005**, *25*, 127–137. [CrossRef]
56. Pelletier, B.R.; Medioli, B.E. *Environmental Atlas of the Beaufort Coastlands*; Natural Resources Canada/ESS/Scientific and Technical Publishing Services: Victoria, BC, Canada, 2014.
57. Giovando, L.F.; Herlinveaux, R.H. *A Discussion of Factors Influencing the Dispersion of Pollutants in the Beaufort Sea*; Pacific Marine Science Report; Institute of Ocean Sciences: Sidney, BC, Canada, 1981; p. 198.
58. Harper, J.R.; Reimer, P.D.; Collins, A.D. *Canadian Beaufort Sea: Physical Shore-Zone Analysis*; Geological Survey of Canada: Ottawa, ON, Canada, 1985; p. 105.
59. Héquette, A.; Desrosiers, M.; Barnes, P.W. Sea Ice Scouring on the Inner Shelf of the Southeastern Canadian Beaufort Sea. *Mar. Geol.* **1995**, *128*, 201–219. [CrossRef]
60. Atkinson, D.E. Observed Storminess Patterns and Trends in the Circum-Arctic Coastal Regime. *Geo-Mar. Lett.* **2005**, *25*, 98–109. [CrossRef]
61. Thomson, J.; Rogers, W.E. Swell and Sea in the Emerging Arctic Ocean. *Geophys. Res. Lett.* **2014**, *41*, 3136–3140. [CrossRef]
62. Pinchin, B.M.; Nairn, R.B.; Philpott, K.L. *Beaufort Sea Coastal Sediment Study: Numerical Estimation of Sediment Transport and Nearshore Profile Adjustment at Coastal Sites in the Canadian Beaufort Sea*; Geological Survey of Canada: Ottawa, ON, Canada, 1985; p. 712.
63. Forbes, D.L.; Taylor, R.B. Ice in the Shore Zone and the Geomorphology of Cold Coasts. *Prog. Phys. Geogr. Earth Environ.* **1994**, *18*, 59–89. [CrossRef]
64. Hill, P.R.; Blasco, S.M.; Harper, J.R.; Fissel, D.B. Sedimentation on the Canadian Beaufort Shelf. *Proc. Can. Cont. Shelf Seabed Symp. CS* **1991**, *11*, 821–842. [CrossRef]
65. Macdonald, R.W.; Solomon, S.M.; Cranston, R.E.; Welch, H.E.; Yunker, M.B.; Gobeil, C. A Sediment and Organic Carbon Budget for the Canadian Beaufort Shelf. *Mar. Geol.* **1998**, *144*, 255–273. [CrossRef]
66. Yang, D.; Shi, X.; Marsh, P. Variability and Extreme of Mackenzie River Daily Discharge during 1973–2011. *Quat. Int.* **2015**, *380–381*, 159–168. [CrossRef]
67. Lantuit, H.; Pollard, W.H. Fifty Years of Coastal Erosion and Retrogressive Thaw Slump Activity on Herschel Island, Southern Beaufort Sea, Yukon Territory, Canada. *Geomorphology* **2008**, *95*, 84–102. [CrossRef]
68. Ayles, G.B.; Snow, N.B. Canadian Beaufort Sea 2000: The Environmental and Social Setting. *Arctic* **2002**, *55*, 4–17. [CrossRef]
69. Obu, J.; Lantuit, H.; Fritz, M.; Pollard, W.H.; Sachs, T.; Günther, F. Relation between Planimetric and Volumetric Measurements of Permafrost Coast Erosion: A Case Study from Herschel Island, Western Canadian Arctic. *Polar Res.* **2016**, *35*, 30313. [CrossRef]
70. Radosavljevic, B.; Lantuit, H.; Plessen, B.; Knoblauch, C. *Granulometry and Bulk Geochemistry of Nearshore Sediments, Herschel Island, Yukon Territory, Canada*; Pangaea: Bremerhaven, Germany, 2016. [CrossRef]
71. Radosavljevic, B. *Tools for Statistical Evaluation and Exploration of Granulometric and Bulk Geochemical Data*; GFZ Data Services: Potsdam, Germany, 2018. [CrossRef]
72. Folk, R.L.; Ward, W.C. Brazos River Bar: A Study in the Significance of Grain Size Parameters. *J. Sediment. Petrol.* **1957**, *27*, 3–26. [CrossRef]
73. Krumbein, W.C.; Pettijohn, F.J. *Manual of Sedimentary Petrography*; Appleton-Century-Crofts: New York, NY, USA, 1938; Volume 549.
74. Blott, S.J.; Pye, K. GRADISTAT: A Grain Size Distribution and Statistics Package for the Analysis of Unconsolidated Sediments. *Earth Surf. Process. Landf.* **2001**, *26*, 1237–1248. [CrossRef]
75. Meyers, P.A. Preservation of Elemental and Isotopic Source Identification of Sedimentary Organic Matter. *Chem. Geol.* **1994**, *114*, 289–302. [CrossRef]
76. Stein, R.; Macdonald, R.W. Organic Carbon Budget: Arctic Ocean vs. Global Ocean. In *The Organic Carbon Cycle in the Arctic Ocean*; Stein, R., Macdonald, R.W., Eds.; Springer: Berlin/Heidelberg Germany, 2004; pp. 315–322.
77. Tanski, G.; Lantuit, H.; Ruttor, S.; Knoblauch, C.; Radosavljevic, B.; Strauss, J.; Wolter, J.; Irrgang, A.M.; Ramage, J.; Fritz, M. Transformation of Terrestrial Organic Matter along Thermokarst-Affected Permafrost Coasts in the Arctic. *Sci. Total Environ.* **2017**, *581–582*, 434–447. [CrossRef] [PubMed]

78. Obu, J.; Lantuit, H.; Myers-Smith, I.; Heim, B.; Wolter, J.; Fritz, M. Effect of Terrain Characteristics on Soil Organic Carbon and Total Nitrogen Stocks in Soils of Herschel Island, Western Canadian Arctic. *Permafr. Periglac. Process.* **2015**, *28*, 92–107. [CrossRef]
79. Efron, B.; Tibshirani, R. Bootstrap Methods for Standard Errors, Confidence Intervals, and Other Measures of Statistical Accuracy. *Stat. Sci.* **1986**, *1*, 54–75. [CrossRef]
80. *R Core Team R: A Language and Environment for Statistical Computing*; R Foundation for Statistical Computing: Vienna, Austria, 2018.
81. Radosavljevic, B. *Workboat Passage Bathymetry Isobaths*; Pangaea: Bremerhaven, Germany, 2018. [CrossRef]
82. Ramage, J.L.; Konopczak, A.M.; Herzschuh, U.; Morgenstern, A.; Couture, N.; Lantuit, H. *Coastal Retrogressive Thaw Slumps along the Yukon Coast (Canada), Link to Shapefile*; Pangaea: Bremerhaven, Germany, 2016. [CrossRef]
83. Fritz, M.; Wolter, J.; Rudaya, N.; Palagushkina, O.; Nazarova, L.; Obu, J.; Rethemeyer, J.; Lantuit, H.; Wetterich, S. Holocene Ice-Wedge Polygon Development in Northern Yukon Permafrost Peatlands (Canada). *Quat. Sci. Rev.* **2016**, *147*, 279–297. [CrossRef]
84. Klein, K.P.; Lantuit, H.; Heim, B.; Fell, F.; Doxaran, D.; Irrgang, A.M. Long-Term High-Resolution Sediment and Sea Surface Temperature Spatial Patterns in Arctic Nearshore Waters Retrieved Using 30-Year Landsat Archive Imagery. *Remote Sens.* **2019**, *11*, 2791. [CrossRef]
85. Reimnitz, E.; Toimil, L.; Barnes, P. Arctic Continental Shelf Morphology Related to Sea-Ice Zonation, Beaufort Sea, Alaska. *Mar. Geol.* **1978**, *28*, 179–210. [CrossRef]
86. Smith, C.A.S.; Kennedy, C.E.; Hargrave, A.E.; McKenna, K.M. *Soil and Vegetation of Herschel Island, Yukon Territory. Yukon Soil Survey Report, Vol. 1. Land Resource Research Centre*; Research Branch, Agriculture Canada: Ottawa, ON, Canada, 1989.
87. Grotheer, H.; Meyer, V.; Riedel, T.; Pfalz, G.; Mathieu, L.; Hefter, J.; Gentz, T.; Lantuit, H.; Mollenhauer, G.; Fritz, M. Burial and Origin of Permafrost-Derived Carbon in the Nearshore Zone of the Southern Canadian Beaufort Sea. *Geophys. Res. Lett.* **2020**, *47*, e2019GL085897. [CrossRef]
88. Visher, G.S. Grain-Size Distributions and Depositional Processes. *J. Sediment. Petrol.* **1969**, *39*, 1074–1106.
89. Kempema, E.W.; Reimnitz, E.; Barnes, P.W. Sea Ice Sediment Entrainment and Rafting in the Arctic. *J. Sediment. Res.* **1989**, *59*, 308–317. [CrossRef]
90. Bauch, H.A.; Kassens, H.; Naidina, O.D.; Kunz-Pirrung, M.; Thiede, J. Composition and Flux of Holocene Sediments on the Eastern Laptev Sea Shelf, Arctic Siberia. *Quat. Res.* **2001**, *55*, 344–351. [CrossRef]
91. Fahl, K.; Stein, R. Modern Organic Carbon Deposition in the Laptev Sea and the Adjacent Continental Slope: Surface Water Productivity vs. Terrigenous Input. *Org. Geochem.* **1997**, *26*, 379–390. [CrossRef]
92. Martens, J.; Romankevich, E.; Semiletov, I.; Wild, B.; van Dongen, B.; Vonk, J.; Tesi, T.; Shakhova, N.; Dudarev, O.V.; Kosmach, D.; et al. CASCADE–The Circum-Arctic Sediment CArbon DatabasE. *Earth Syst. Sci. Data* **2021**, *13*, 2561–2572. [CrossRef]
93. Wijsman, J.; Herman, P.; Gomoiu, M. Spatial Distribution in Sediment Characteristics and Benthic Activity on the Northwestern Black Sea Shelf. *Mar. Ecol. Prog. Ser.* **1999**, *181*, 25–39. [CrossRef]
94. Burdige, D.J. Burial of Terrestrial Organic Matter in Marine Sediments: A Re-Assessment. *Glob. Biogeochem. Cycles* **2005**, *19*. [CrossRef]
95. Keil, R.G.; Tsamakis, E.; Fuh, C.B.; Giddings, J.C.; Hedges, J.I. Mineralogical and Textural Controls on the Organic Composition of Coastal Marine Sediments: Hydrodynamic Separation Using SPLITT-Fractionation. *Geochim. Cosmochim. Acta* **1994**, *58*, 879–893. [CrossRef]
96. Pedrosa-Pàmies, R.; Sanchez-Vidal, A.; Calafat, A.; Canals, M.; Durán, R. Impact of Storm-Induced Remobilization on Grain Size Distribution and Organic Carbon Content in Sediments from the Blanes Canyon Area, NW Mediterranean Sea. *Prog. Oceanogr.* **2013**, *118*, 122–136. [CrossRef]
97. Tesi, T.; Miserocchi, S.; Goñi, M.A.; Langone, L. Source, Transport and Fate of Terrestrial Organic Carbon on the Western Mediterranean Sea, Gulf of Lions, France. *Mar. Chem.* **2007**, *105*, 101–117. [CrossRef]
98. Lantuit, H.; Pollard, W.H.; Couture, N.; Fritz, M.; Schirrmeister, L.; Meyer, H.; Hubberten, H.-W. Modern and Late Holocene Retrogressive Thaw Slump Activity on the Yukon Coastal Plain and Herschel Island, Yukon Territory, Canada. *Permafr. Periglac. Process.* **2012**, *23*, 39–51. [CrossRef]
99. Grosse, G.; Harden, J.; Turetsky, M.; McGuire, A.D.; Camill, P.; Tarnocai, C.; Frolking, S.; Schuur, E.A.G.; Jorgenson, T.; Marchenko, S.; et al. Vulnerability of High-Latitude Soil Organic Carbon in North America to Disturbance. *J. Geophys. Res. Biogeosci.* **2011**, *116*, G00K06. [CrossRef]
100. Dutta, K.; Schuur, E.A.G.; Neff, J.C.; Zimov, S.A. Potential Carbon Release from Permafrost Soils of Northeastern Siberia. *Glob. Chang. Biol.* **2006**, *12*, 2336–2351. [CrossRef]
101. Rivkina, E.; Gilichinsky, D.; Wagener, S.; Tiedje, J.; McGrath, J. Biogeochemical Activity of Anaerobic Microorganisms from Buried Permafrost Sediments. *Geomicrobiol. J.* **1998**, *15*, 187–193. [CrossRef]
102. Schuur, E.A.G.; Vogel, J.G.; Crummer, K.G.; Lee, H.; Sickman, J.O.; Osterkamp, T.E. The Effect of Permafrost Thaw on Old Carbon Release and Net Carbon Exchange from Tundra. *Nature* **2009**, *459*, 556. [CrossRef] [PubMed]
103. Schädel, C.; Schuur, E.A.G.; Bracho, R.; Elberling, B.; Knoblauch, C.; Lee, H.; Luo, Y.; Shaver, G.R.; Turetsky, M.R. Circumpolar Assessment of Permafrost C Quality and its Vulnerability over Time using Long-Term Incubation Data. *Glob. Chang. Biol.* **2014**, *20*, 641–652. [CrossRef]

104. Mann, P.J.; Eglinton, T.I.; McIntyre, C.P.; Zimov, N.; Davydova, A.; Vonk, J.E.; Holmes, R.M.; Spencer, R.G.M. Utilization of Ancient Permafrost Carbon in Headwaters of Arctic Fluvial Networks. *Nat. Commun.* **2015**, *6*, 7856. [CrossRef] [PubMed]
105. Fritz, M.; Opel, T.; Tanski, G.; Herzschuh, U.; Meyer, H.; Eulenburg, A.; Lantuit, H. Dissolved Organic Carbon (DOC) in Arctic Ground Ice. *Cryosphere Discuss.* **2015**, *9*, 77–114. [CrossRef]
106. Zimov, S.A.; Davydov, S.P.; Zimova, G.M.; Davydova, A.I.; Schuur, E.A.G.; Dutta, K.; Chapin, F.S. Permafrost Carbon: Stock and Decomposability of a Globally Significant Carbon Pool. *Geophys. Res. Lett.* **2006**, *33*, L20502. [CrossRef]
107. Dou, F.; Ping, C.-L.; Guo, L.; Jorgenson, T. Estimating the Impact of Seawater on the Production of Soil Water-Extractable Organic Carbon during Coastal Erosion. *J. Environ. Qual.* **2008**, *37*, 2368–2374. [CrossRef]
108. Magen, C.; Chaillou, G.; Crowe, S.A.; Mucci, A.; Sundby, B.; Gao, A.; Makabe, R.; Sasaki, H. Origin and Fate of Particulate Organic Matter in the Southern Beaufort Sea–Amundsen Gulf Region, Canadian Arctic. *Estuar. Coast. Shelf Sci.* **2010**, *86*, 31–41. [CrossRef]
109. Belicka, L.L.; Harvey, H.R. The Sequestration of Terrestrial Organic Carbon in Arctic Ocean Sediments: A Comparison of Methods and Implications for Regional Carbon Budgets. *Geochim. Cosmochim. Acta* **2009**, *73*, 6231–6248. [CrossRef]
110. Tyson, R.V. *Sedimentary Organic Matter: Organic Facies and Palynofacies*; Chapman & Hall: London, UK; New York, NY, USA, 1995; ISBN 0-412-36350-X.
111. Fritz, M.; Wetterich, S.; Meyer, H.; Schirrmeister, L.; Lantuit, H.; Pollard, W.H. Origin and Characteristics of Massive Ground Ice on Herschel Island (Western Canadian Arctic) as Revealed by Stable Water Isotope and Hydrochemical Signatures. *Permafr. Periglac. Process.* **2011**, *22*, 26–38. [CrossRef]
112. Schubert, C.J.; Calvert, S.E. Nitrogen and Carbon Isotopic Composition of Marine and Terrestrial Organic Matter in Arctic Ocean Sediments: Implications for Nutrient Utilization and Organic Matter Composition. *Deep Sea Res. Part Oceanogr. Res. Pap.* **2001**, *48*, 789–810. [CrossRef]
113. Burdige, D.J. Preservation of Organic Matter in Marine Sediments: Controls, Mechanisms, and an Imbalance in Sediment Organic Carbon Budgets? *Chem. Rev.* **2007**, *107*, 467–485. [CrossRef] [PubMed]
114. Shepard, F.P. Nomenclature Based on Sand-Silt-Clay Ratios. *J. Sediment. Res.* **1954**, *24*, 151. [CrossRef]